Mem. S.A.It. Vol. 76, 842

Memorie della

On the effect of photospheric magnetic fields on solar surface brightness

Results of radiative MHD simulations

A. Vögler

Max-Planck-Institut für Sonnensystemforschung, Max-Planck-Strasse 2, 37191 Katlenburg-Lindau, Germany * e-mail: voegler@mps.mpg.de

Abstract.
Magnetic features in the solar surface layers are assumed to be a main cause for solar irradiance variations on timescales of the solar cycle and shorter. Realistic radiative MHD simulations of photospheric magneto-convection allow us to study the interaction between magnetic features, convective flows and radiation in detail and help to understand the physical mechanisms underlying irradiance variations, whilst at the same time allowing direct comparison with observations. We report on a series of local-box MHD simulations covering magneto-convection in the photosphere from quiet Sun to strong plage conditions. We find that for average magnetic field strengths corresponding to plage or facular regions, the total emergent radiation flux is increased by 2 - 3 % relative to quiet Sun conditions, mainly as a result of increased radiative losses along inclined rays from the hot walls of faculae. For stronger average fields, the radiative energy output drops below quiet Sun levels, partly due to a darker appearance of magnetic features near disk center, partly due to reduced granule brightness. The simulations underline that the modification of convective and radiative energy transport in the photosphere due to surface magnetism is a viable mechanism for solar irradiance variations. The center-to-limb variation of bolometric intensity and facular contrast show good agreement with observations, suggesting that realistic radiative MHD simulations can be useful for refined models of solar irradiance variations.

Key words. MHD – Sun: magnetic fields – Sun: photosphere – Sun: activity – Sun: faculae, plages

1. Introduction

The total solar irradiance is known to change on a variety of timescales. Empirical models show that irradiance variations are strongly correlated with changes of the amount and distribution of magnetic flux on the solar surface (e.g. Krivova et al. 2003). In these models changes in irradiance are mainly determined by the darkening effect of sunspots and a brightness enhancement due to faculae. However, these models involve at least one adjustable parameter so that their predictive and explanatory power is somewhat limited. In this context, realistic simulations of solar surface magne-

* *Present address:* High Altitude Observatory, National Center for Atmospheric Research,3080 Center Green Dr., Boulder, C0 80301, USA

toconvection serve a twofold purpose: Firstly, they allow us to investigate the physical mechanism behind changes in brightness and radiation flux, thus providing the theoretical underpinning for a connection between surface magnetism and irradiance. Secondly, a systematic study of solar surface simulations will contribute to our knowledge of the photometric properties of network and plage magnetic fields and may provide accurate input parameters for improved irradiance models.

State-of-the-art radiative MHD simulations of photospheric magnetoconvection have reached a high level of realism and have been very successful in reproducing and explaining surface features like G-Band bright points (Schüssler et al. 2003, Shelyag et al. 2004) or facular brightenings (Keller et. al 2004, Carlsson et al. 2004). In this paper we follow this approach of realistic modelling. We present a series of magnetoconvection simulations covering quiet Sun, network and plage conditions and analyze the dependence of average photometric properties, including the emergent radiation flux and center-to-limb variation of intensity and facular contrast, on the average magnetic field strength.

2. Simulation Setup

Using the MURaM code (Vögler et al. 2005), we carried out a series of radiative MHD simulations with average field strengths ranging from nonmagnetic, purely hydrodynamic convection to magnetoconvection under conditions corresponding to strong plage.

The MURaM code solves the time-dependent MHD equations for a compressible and partially ionized plasma including a non-grey LTE radiative transfer based on multi-group frequency binning. The bottom boundary condition allows free in- and outflow of matter, maintaining a constant total mass in the box, while the top boundary is closed. The magnetic field is assumed to be vertical at the top and bottom boundaries, the footpoints of fieldlines are allowed to move freely. The horizontal directions are taken to be periodic. A detailed description of the code and the numerical methods can be found in Vögler (2003), Vögler et al. (2005) and Vögler, Bruls & Schüssler (2004). The computational domain extends 1400 km in the vertical direction and 6000 km in both horizontal directions, with a resolution of $100 \times 288 \times 288$ grid points. The level of average continuum (500 nm) optical depth unity, $\langle \tau_{500} \rangle = 1$, is located 500 - 600 km below the upper boundary.

The results presented in Sec. 3 are based on five different simulation runs. Apart from a nonmagnetic reference run, four magnetic runs with varying amount of magnetic flux were carried out. The magnetic runs were started by introducing a homogeneous, vertical magnetic field of strength B_0 into fully developed convection. The values chosen for B_0 are 50 G (comparable to quiet Sun network), 200 G, 400 G (typical values for plage regions), and 800 G. In order to study how the magnetic field affects the energy transport and the total radiative energy output, we specified the entropy density of the fluid entering the simulation domain from below, letting the total energy flux through the system adjust itself according to the conditions of a given simulation run. Assuming that the entropy throughout the upflowing parts of the convection zone is essentially constant, with inhomogeneities efficiently smoothed out by the strong expansion of rising fluid parcels in a strongly stratified system, we chose the entropy density to be uniform across the upflow regions at the lower boundary and independent of B_0. The entropy of inflowing material was calibrated such that the radiative energy flux of the nonmagnetic run on average roughly equals[1] the solar value $F_\odot = 6.3\,10^{10}\,\mathrm{erg\,cm^{-2}\,s^{-1}}$. After several convective turnover times the simulations reached a statistically stationary state. All simulation runs were continued until approximately 150 minutes of simulated solar time in the stationary phase were accumulated.

[1] We found the outgoing radiative flux averaged over the statistically stationary phase to be about 1% below the nominal value $F_\odot$. Since we are only interested in relative differences between different simulation runs, this deviation is largely irrelevant.

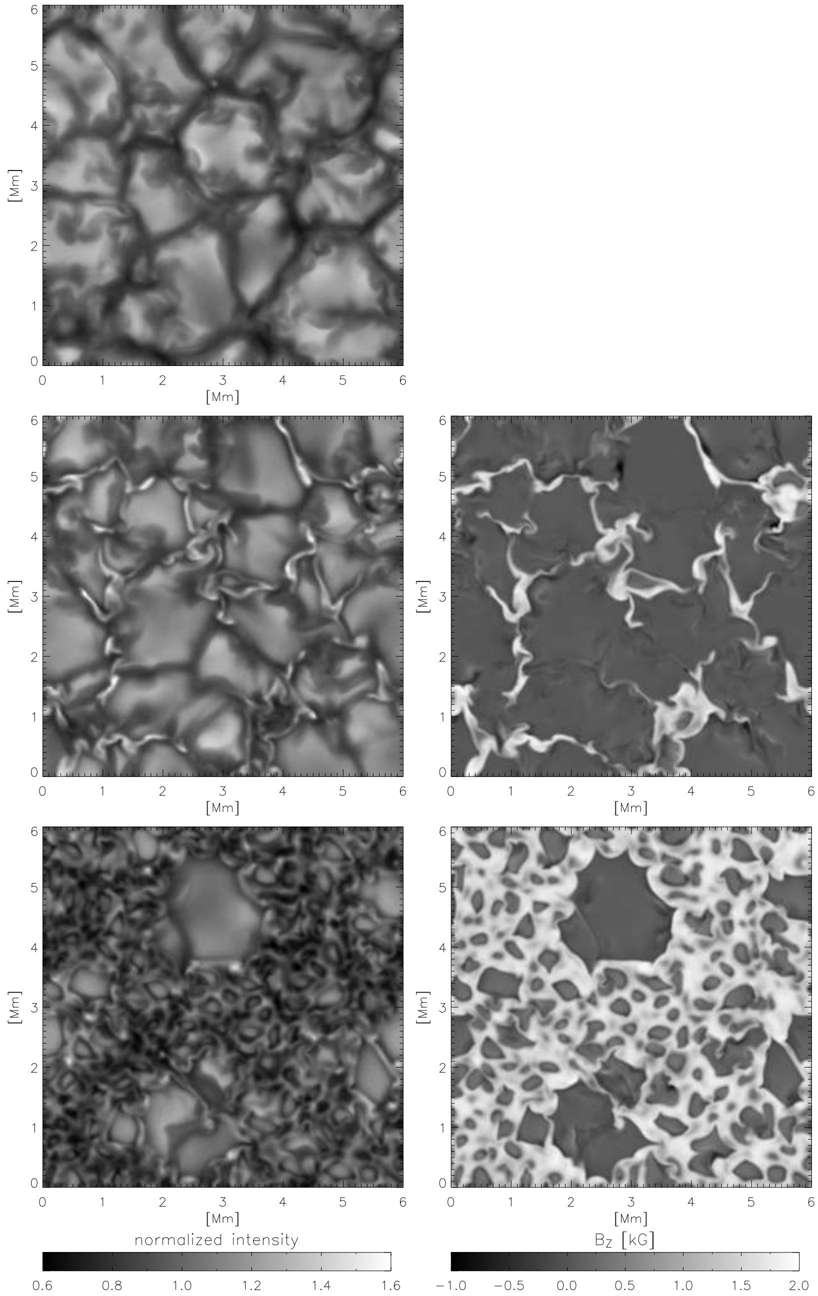

Fig. 1. Left column: Maps of bolometric brightness for representative simulation snapshots with $B_0 = 0$ (top), 200 G (middle), and 800 G (bottom). The same greyscale was used for all three maps. Right column: corresponding horizontal cuts of the vertical magnetic field strength near $\langle\tau_{500}\rangle = 1$. Strong fields appear white, dark grey regions are essentially field-free.

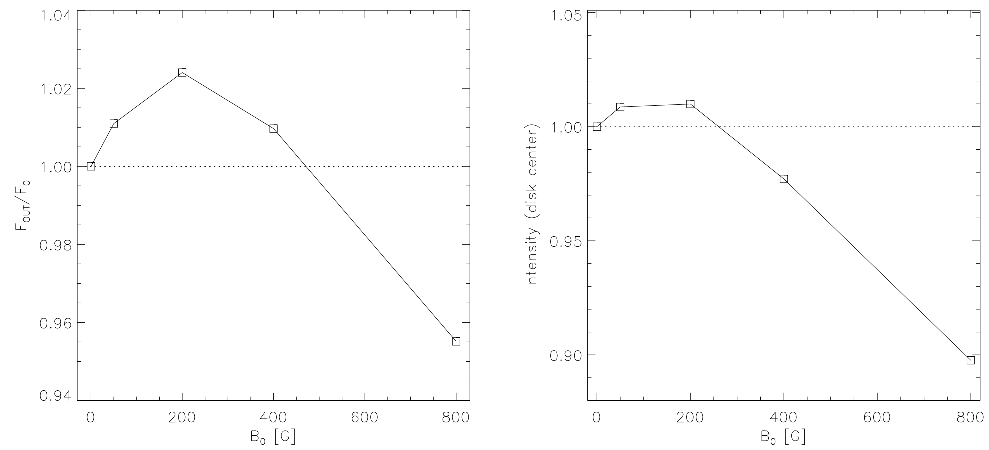

Fig. 2. Spatio-temporal average of the outgoing (angle-integrated) bolometric radiation flux (left panel) and of the bolometric disk-center intensity (right panel), as a function of the average field strength, B_0. Both curves are normalized with the values for the non-magnetic case.

3. Results

Fig. 1 gives an impression of the morphology of photospheric magnetoconvection for different values of the average magnetic field strength. The upper panel shows the granulation pattern of nonmagnetic convection. For B_0 = 200 G (middle row), the granulation appears disturbed, with on average smaller granules ("abnormal granulation"). Most of the magnetic field gets swept into the intergranular downflow network and is amplified to field strength of 1.5 - 2 kG near the visible surface of optical depth unity. The kilogauss fields (appearing white on the magnetic maps of Fig.1) are organized in a network of thin sheet-like structures which appear bright in the intensity image. Occasionally, dark micropores form at downflow vertices. With increasing amount of magnetic flux, the convection becomes less vigorous and the horizontal scale of granulation decreases. The simulation with B_0 = 800 G (bottom row) is an example of severely disturbed granulation. With an average field strength far beyond typical values for solar plage, this case illustrates the transition to the magnetically dominated regime of magnetoconvection. Here, the dynamic backreaction of the magnetic field leads to the formation of numerous small, weakly magnetized upflow plumes with typical diameters of a few hundred kilometers. Embedded into this background of strong field interspersed with small-scale flows are a small number of larger upflows roughly the size of ordinary granules.

The left panel of Fig. 2 shows the angle-integrated bolometric radiation flux at the top of the computational domain (i.e. the energy per unit area and unit time radiated by the model) averaged over space and time as a function of the average magnetic field strength B_0 in the five simulation runs. For the cases with B_0 = 50, 200, and 400 G, the radiation flux is larger than in the nonmagnetic run, the flux excess reaching a maximum of approximately 2.5 % for the 200 G run. In the 800 G case, on the other hand, the radiation flux is reduced by about 4.5 %.

The bolometric brightness at disk center (right panel of Fig. 2) is is enhanced by approximately 1% for the cases with B_0 = 50 and 200 G. For larger B_0 the values drop clearly, reaching a brightness reduction of 10% for the 800 G case. In general, for all four magnetic runs the normalized disk-center intensities appear to have lower values than the normalized flux integrated over the upper hemipshere, indicating a modified angular dependence of the

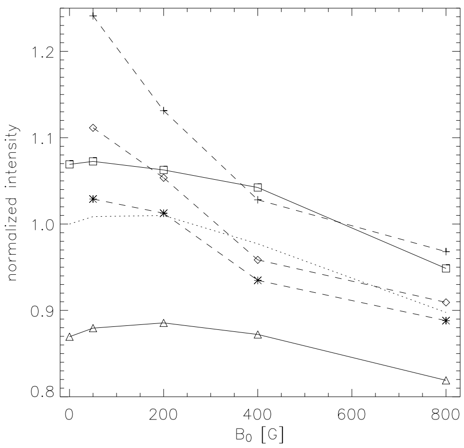

Fig. 3. Average disk-center intensity as a function of the average field strength B_0. The curves correspond to averages taken over granules (solid line, squares), downflow lanes (solid line, triangles), and regions with B_z exceeding 500 G (dashed, asterisks), 1.0 kG (dashed, diamonds), and 1.5 kG (dashed, crosses) at $\langle\tau_{500}\rangle = 1$. The dotted line shows the average over the whole area (same as Fig. 2, right panel) for comparison. All values are relative to the average disk-center intensity of the non-magnetic run.

radiative energy transport, as is discussed in more detail below.

In order to gain insight into how the brightness variations come about, we decompose the disk-center brightness maps into three constituents, based on field strength and vertical velocity at a height level corresponding to $\langle\tau_{500}\rangle = 1$: granular upflows (areas with $|B_z| < 500$ G and $v_z > 0$), intergranular downflow lanes ($|B_z| < 500$ G and $v_z < 0$) , and magnetic flux concentrations ($|B_z| > 500$ G). Fig. 3 shows the average brightness of granules, lanes and magnetic fields, all taken relative to the average brightness of the nonmagnetic simulation run. For the 50 G and 200 G cases, the brightness of granules is only weakly affected by the magnetic field. However, for $B_0 > 50$ G there is a decrease of of granule brightness which amounts to about 10 % for the simulation with $B_0 = 800$ G . The darkening of granules with increasing average field strength can be understood as a result of hampered convective energy transport in the presence of magnetic fields. Accordingly, one finds that kinetic energy and rms flow velocities near the visible surface decrease notably with increasing B_0. This result suggests that the inhibition of the convective energy transport by magnetic fields has a significant effect on the radiative energy output for photospheric regions with average flux densities beyond 200 G. Interestingly, the brightness of downflow lanes in the 50, 200, and 400 G cases is somewhat larger than in the case $B_0 = 0$. A possible explanation may lie in the fact that the magnetic flux concentrations embedded in the downflow network flare out with height, so in the upper photosphere the line of sight of downflow lanes partially runs through the partially evacuated, optically thin magnetic canopy. As a result one can look into deeper, hotter layers, not unlike the hot wall effect that leads to facular brightenings (e.g. Spruit 1976, Keller et al. 2004). For $B_0 > 200$ G the lane brightness follows the systematic downward trend of the granules. A more detailed analysis of the thermodynamic structure and the conditions under which the intensity forms is required to clarify the mechanisms at work here.

The three dashed curves in Fig. 3 show the average brightness of magnetic flux concentrations, with three different values (0.5, 1.0, and 1.5 kG) for the threshold field strength at $\langle\tau_{500}\rangle = 1$. Independently of B_0 one finds that the average brightness increases with increasing threshold level, i.e. the strongest fields appear brightest. This results from the fact that the level of optical depth unity is depressed in regions of strong field because of the higher degree of evacuation, thus exposing hotter material. All three curves exhibit a clear downward trend with growing B_0. This can be understood as a consequence of the tendency of magnetoconvection to form larger magnetic structures as the average flux density increases. The radiated energy coming from magnetic structures is mainly supplied by lateral channelling of hot-wall radiation (convective transport inside the strong fields is negligible). With growing filling factor and size of strong field features, the thermal structure of strong fields has to adjust in order to maintain a balance be-

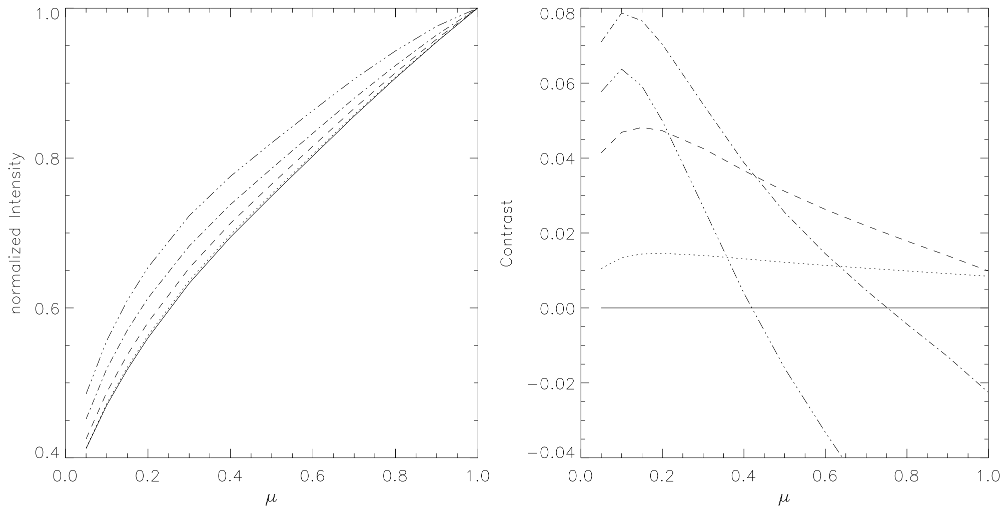

Fig. 4. Left panel: Center-to-limb variation of the bolometric intensity for the five simulation runs with an average field strength of 0 (solid line), 50 G (dotted), 200 G (dashed), 400 G (dash-dotted), and 800 G (triple-dot-dashed). All curves are normalized individually to the value at disk center. Right panel: Center-to-limb variation of the contrast, $(I(\mu) - I_0(\mu))/I_0(\mu)$, where $I_0(\mu)$ is the angle-dependent intensity of the of the nonmagnetic simulation run.

tween the horizontal energy input through the walls and the radiative losses in the vertical direction, resulting in lower brightness. As a comparison with the brightness averaged over the whole area (dotted line and right panel of Fig. 2) shows, flux concentrations with field strengths larger that 1.5 kG on average stand out as bright features for all values of B_0. For the 50 G and 200 G cases, the values for kilogauss fields significantly exceed the average "quiet Sun" ($B_0 = 0$) disk-center brightness. Their contribution to the brightness enhancement is however limited because of the small filling factors of 1.8% and 9.3%, respectively.

As mentioned above, the different dependence on B_0 of radiation flux and disk-center intensity is indicative of a modified angular distribution of the radiation field in the presence of a magnetic field. This effect is illustrated in the left panel of Fig. 4 which shows the center-to-limb variation (CLV) of the bolometric intensity relative to disk center, $I_{\rm bol}(\mu)/I_{\rm bol}(\mu = 1)$, with $\mu = \cos\theta$, where θ is the heliocentric angle. All five curves show limb darkening. However, for any given μ the intensity relative to disk center increases with B_0, indicating that higher average magnetic field strengths lead to enhanced radiative leakage from the hot walls of faculae along slanted rays. A comparison of the curves for 0 and 50 G with the measured broadband light CLV from the Solar Bolometric Imager (Foukal et al. 2004) shows good agreement to within roughly one percent for $\mu \geq 0.2$ (see Fig. 5), which underlines the high degree of realism of the simulations. The curve for $B_0 = 50$ G seems to match the observation slightly better, which is not completely surprising if one keeps in mind that the quiet Sun is not entirely field-free. Based on spectropolarimetric measurements, values for the total unsigned quiet-Sun magnetic flux of the order of several ten Gauss have been suggested (see e.g. Khomenko et al. 2005 and references therein), so it may well be that the 50 G simulation is a better model for the quiet Sun than a completely nonmagnetic one. For heliocentric angles closer to the limb than $\mu = 0.2$ the simulated CLV falls off more steeply and is in good agreement with the CLV synthesized from the monochromatic measurements by Neckel & Labs (1994) (dashed line in Fig. 5, see Foukal et al. 2004 for further details).

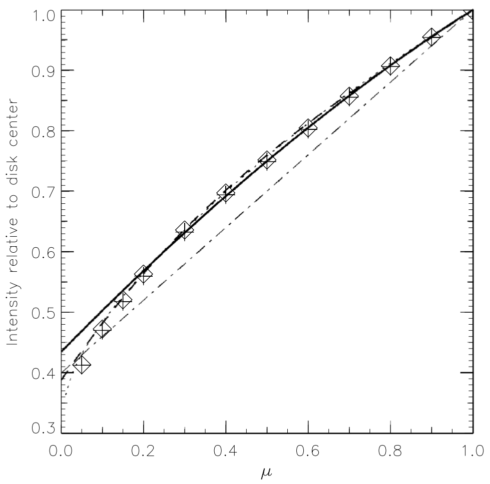

Fig. 5. This viewgraph was adapted from the paper by Foukal et al. (2004). The photospheric limb darkening measured in broadband light with SBI is shown as solid curve. The result from the nonmagnetic simulation (crosses) and the simulation with $B_0 = 50$ G (diamonds) have been added for comparison.

The CLV of the contrast, $(I(\mu) - I_0(\mu))/I_0(\mu)$, where $I_0(\mu)$ is the angle-dependent intensity of the nonmagnetic model, is shown in Fig. 4, right panel. Obviously, the CLV of the contrast depends strongly on the amount of magnetic flux in the simulation. For small B_0 the contrast varies relatively weakly with μ and is always positive. For large B_0 the contrast is negative at disk center, grows strongly as a function of μ and is positive near the limb. Over a large range of values for B_0 the maximum contrast obtained increases with B_0, beyond $B_0 = 400$ G it drops again but seems to be less sensitive to a further increase of the average magnetic field strength. The picture obtained here exhibits many qualitative similarities with the MDI-based contrast measurements by Ortiz et al. (2002). The most striking difference is the heliocentric angle where the maximum contrast occurs. In our simulations, the contrast increases monotonously up to at least $\mu = 0.2$ for small B_0 and continues growing towards the limb for large B_0, while the contrasts in the study by Ortiz et al. (2002) generally reach their maximum closer to disk center. A possible explanation for this discrepancy may lie in the fact that in the latter study the magnetic field strength is extracted from the magnetogram signal averaged over an MDI pixel which carries no information about the spatial distribution of magnetic flux within the resolution element. Thus different magnetic configurations with the same magnetogram signal but potentially very different CLV are grouped into the same field-strength bin, which may have a nivellating effect on the contrast. One should also keep in mind that the CLV of the contrast may be wavelength dependent, so caution is adviced when comparing the synthesized bolometric intensities with results based on MDI continuum measurements.

4. Summary and Conclusions

We have carried out a series of photospheric magnetoconvection simulations with the aim of studying the dependence of photospheric energy transport and photometric properties on the average magnetic field strength. The main results of a first, preliminary analysis can be summarized as follows:

- For average field strength corresponding to plage regions (200 - 300 G), the total radiative energy output is increased by 2 - 3 % relative to nonmagnetic convection. For average field strengths beyond about 500 G, the total emittance is reduced.
- With increasing amount of magnetic flux, the center-to-limb variation of the bolometric intensity flattens, and radiative energy transport along inclined rays becomes more important.
- The decrease in emittance for large average field strengths is partly due to a lower intensity of kilogauss flux concentrations near disk center, and partly due to reduced granule brightness.
- The CLV of the bolometric contrast (relative to quiet Sun) of the magnetoconvection

models depends strongly on the average field strength: for small field strengths corresponding to network, the contrast is positive for all heliocentric angles, for strong plage conditions the contrast is negative at disk center and positive near the limb.

The finding that the radiative energy output in simulations of plage or facular regions is significantly enhanced supports the hypothesis that surface magnetism is a main cause of short-term solar irradiance variations. The good agreement of the CLV of intensity and facular contrast with observations suggests that simulations of this kind may be useful as a basis for a refined modelling of total solar irradiance variations. The analysis presented here is still preliminary in nature. In a more in-depth analysis, questions like the wavelength dependence of photometric properties and the effects of numerical resolution will be addressed.

Acknowledgements. I would like to thank M. Schüssler and S. K. Solanki for helpful suggestions and comments.

References

Carlsson, M., Stein, R. F., Nordlund, Å., & Scharmer, G. B. 2004, ApJ, 610, L137

Foukal, P., Bernasconi, P., Eaton, H., & Rust, D. 2004, ApJ, 611, L57

Keller, C. U., Schüssler, M., Vögler, A., Zakharov, V. 2004, ApJ, 607, L59

Khomenko, E. V., Martínez González, M. J., Collados, M., Vögler, A., Solanki, S. K., Ruiz Cobo, B., & Beck, C. 2005, A&A, 436, L27

Krivova, N. A., Solanki, S. K., Fligge, M., & Unruh, Y. C. 2003, A&A, 399, L1

Neckel, H., & Labs, D. 1994, Sol. Phys., 153, 91

Ortiz, A., Solanki, S. K., Domingo, V., Fligge, M., & Sanahuja, B. 2002, A&A, 388, 1036

Schüssler, M., Shelyag, S., Berdyugina, S., Vögler, A., Solanki, S. K. 2003, ApJ, 597, L173

Shelyag, S., Schüssler, M., Solanki, S. K., Berdyugina, S. V., Vögler, A. 2004, A&A, 427, 335

Spruit, H. C. 1976, Sol. Phys., 50, 269

Vögler, A. 2003, PhD thesis, Göttingen University, http://webdoc.sub.gwdg.de/diss/2004/voegler/voegler.pdf

Vögler, A., Bruls, J. H. M. J., Schüssler, M. 2004, A&A, 421, 741

Vögler, A., Shelyag, S., Schüssler, M., Cattaneo, F., Emonet, T., Linde, T. 2005, A&A, 429, 335